Operation of an Annular Helicon Plasma Source

Douglas D. Palmer[1] and Mitchell L. R. Walker[2]
High-Power Electric Propulsion Laboratory
Department of Aerospace Engineering
Georgia Institute of Technology, Atlanta, GA, 30332 USA
Phone: 404-385-2757
Fax: 404-894-2760

The plasma parameters of a nominally 1.5-kW annular helicon plasma source are experimentally measured. All experiments are performed in the Georgia Institute of Technology Vacuum Test Facility at pressures below 5.0 x 10^{-5} Torr-Ar, and 5.6 x 10^{-5} Torr-Xe. The study characterizes the source over a range of applied RF frequencies (2-15 MHz), for both argon and xenon mass flow rates (1 – 4 mg/s), magnetic field strengths (0 - 400 Gauss), and RF forward power settings (100 - 1500 W). The ion number density, electron temperature, and electron energy distribution function (EEDF) are measured at several radial and axial locations within the annulus at each operating condition with a Hiden Analytical RF-compensated Langmuir probe. The peak ion number density is 3.5 x 10^{17} m^{-3} for argon and 2.5 x 10^{17} m^{-3} for xenon. The EEDF peak varies with the RF frequency, from a minimum of 2.2 eV to a maximum of 4.5 eV for argon propellant over the above operating conditions.

Nomenclature

A_p = Langmuir probe collection area
e = electron charge
I_{es} = electron saturation current
k = Boltzmann constant
m_e = electron mass
n_i = ion number density
T_e = electron temperature
V_p = plasma floating potential
γ = plume divergence coefficient
η = device efficiency
ω_{ic} = ion cyclotron frequency
ω_{ec} = electron cyclotron frequency
Λ = electron cyclotron frequency

I. Introduction

Two-stage Hall effect thrusters (HETs), which decouple the ionization stage from the acceleration stage, could achieve a higher efficiency in high-thrust, low-Isp operation than single-stage HETs. The efficiency of an electrostatic acceleration device, which is defined as a ratio of the thrust power to the input power, is expressed as[1]

$$\eta = \frac{P_{thrust}}{P_{input}} = \frac{\eta_u \gamma}{1 + \frac{(\varepsilon + V_{nc})}{V_D}} \tag{1}$$

where η is the propellant utilization efficiency, γ is the plume divergence coefficient, ε is the ionization cost, V_{nc} is the neutralizer coupling voltage, and V_D is the discharge voltage. High thrust-to-power operation requires high

[1] Graduate Student Researcher, Aerospace Engineering, 270 Ferst Drive, Atlanta, GA, 30332, Member AIAA.
[2] Assistant Professor, Aerospace Engineering, 270 Ferst Drive, Atlanta, GA 30332, Member AIAA.

mass flow at a low discharge voltage. However, Eq. 1 shows that the efficiency of thruster decreases at a low discharge voltage because a large fraction of energy is spent on ionization instead of acceleration. A solution to the problem is to replace the DC electron bombardment ionization stage with an efficient ionization source, which decouples the ionization and acceleration mechanisms.[2] Two-stage HETs, which have separate ionization and acceleration stages, have been investigated in the past, but a helicon source has never been used as the ionization stage. [1, 3-14]

A helicon plasma source is a high density, high efficiency plasma source that sustains steady plasma production through absorption and propagation of helicon waves.[15] The wave is launched by sending RF waves along an applied axial magnetic field.[16] Previous works have indicated the wave mode can be identified by jumps in ion saturation current.[17] Helicon mode plasma can also be verified using a B-dot probe to determine the axial and radial wave number.[18] To date, helicon waves have only been excited in cylindrical sources. A cylindrical source is not suitable for the ionization stage of a HET because guiding cylindrical plasma into an annular channel will result in a large plasma loss. However, if a helicon plasma can be excited in a coaxial configuration, the source can directly feed high-density plasma into the acceleration stage of a HET and other coaxial accelerators.[19] The theoretical existence of annularly-bounded helicon waves has been discussed previously.[20]

An annular helicon theoretical model has been developed and trade studies have been performed, indicating the plasma number densities required by a two-stage HET are attainable in this configuration.[21] This work shows that a high density, high efficiency annular helicon plasma source requires dual concentric left-helical antennas to excite the helicon (m=1) mode within the annulus, however experimental verification of helicon wave mode has not been established. The High-Power Electric Propulsion Laboratory (HPEPL) has designed, built, and operated this device, creating plasmas throughout the 2 – 15 MHz frequency and 0 – 450 Gauss ranges. Recent works at HPEPL show the annular helicon is capable of producing high-density plasmas throughout the 7-15 MHz range, but this has yet to be fully characterized.[21, 22] This research effort completes the characterization of the plasma source as a function of axial and radial location, RF forward power, magnetic field, mass flow rate, and RF frequency.

II. Experimental Apparatus

A. Facility

All experiments are performed in the Vacuum Test Facility (VTF), shown schematically in Fig. 1. The VTF is

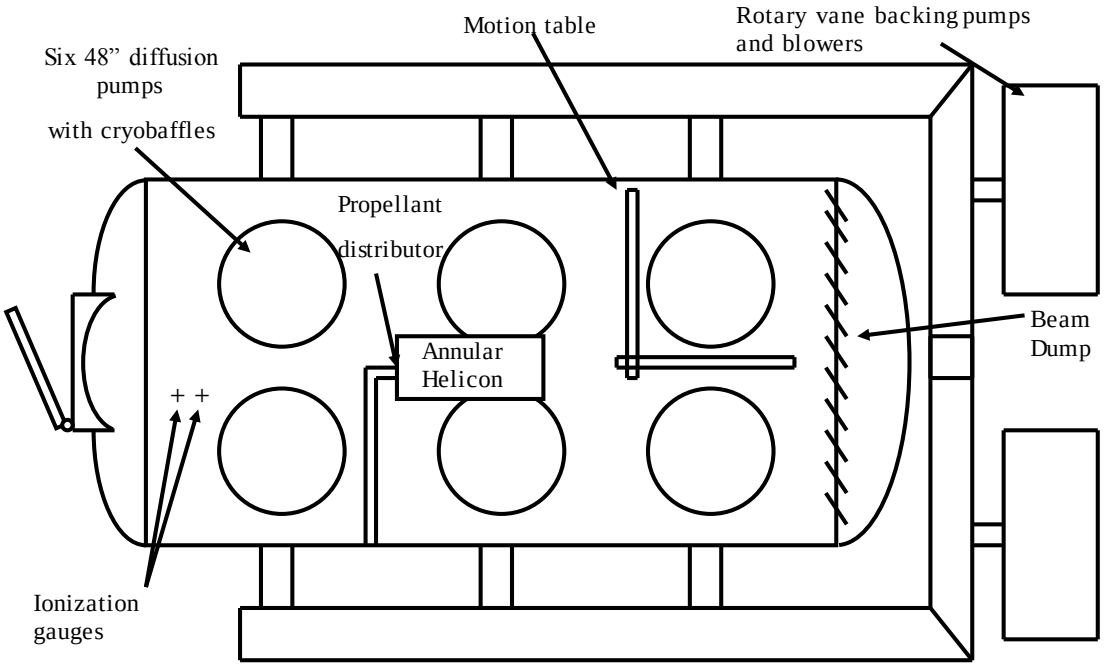

Figure 1. Schematic of Vacuum Test Facility.

a stainless steel vacuum chamber that has a diameter of 4 m and a length of 7 m. Two 3800 CFM blowers and two 495 CFM rotary-vane pumps evacuate the facility to moderate vacuum (30 mTorr). To reach high-vacuum (10^{-7} Torr), the VTF employs six 48" diffusion pumps, with a combined nominal pumping speed of 600,000 l/s on air, 840,000 L/s on hydrogen, and 155,000 l/s on xenon. The VTF pumping speed is varied by changing the number of diffusion pumps in operation. The combined pumping speed of the facility is 600,000 l/s on air and with a base pressure of 1.2×10^{-4} Pa (9.5×10^{-7} Torr).

A Varian model UHV-24 ionization gauge with a Varian senTorr vacuum gauge controller monitors the chamber pressure. The UHV-24 ionization gauge is calibrated for air by the manufacturer. The ionization gauge measures pressure over the range of 10^{-2} Pa (10^{-4} Torr) to 10^{-10} Pa (10^{-12} Torr) with an accuracy of ±20% as reported by Varian.[23] The VTF also utilizes a tubulated Kurt J. Lesker Company (KJLC) model G100TF ionization gauge with a KJLC model IG2200 ionization gauge controller, and a KJLC Accu-Quad residual gas analyzer (RGA), both located on the top of the chamber. The RGA has a detection limit of 5×10^{-14} Torr, and an accuracy of ±10% as reported by KJLC.

Table 1. Operating pressures for mass flow rates of xenon.

Mass flow rate mg/s	Operating Pressure Torr-Xe
0.5	4.3×10^{-5}
1.5	4.8×10^{-5}
2.5	5.2×10^{-5}
3	5.6×10^{-5}

Table 2. Operating pressures for mass flow rates of argon.

Mass flow rate mg/s	Operating Pressure Torr-Ar
0.5	2.0×10^{-5}
1.5	2.4×10^{-5}
2.5	2.7×10^{-5}
3	3.0×10^{-5}

Table 1 and 2 show the VTF operating pressure for each flow rate. Previous investigations show these pressures are lower than typical pressures for helicon experiments.[15, 24, 25] The chamber pressures listed are the indicated pressures from the RGA.

B. Annular Helicon Plasma Source

Figure 2 shows the annular helicon plasma source used in this experiment. The annular ionization chamber is comprised of two concentric Pyrex tubes with inner diameters of 120 mm and 171 mm and thicknesses of 3 mm and 3.5 mm, respectively. A left twist helical pitch antenna is wrapped on the outside of the outer tube, with a separate left twist helical pitch antenna wrapped on the inside of the inner tube. The antennas are constructed from 1/2" wide by 1/8" thick copper strips, and are wrapped in 3M glass cloth electrical tape to prevent direct contact of the plasma with the antennas. The outer antenna has an outer diameter of 186 mm and a length of 192.7 mm. The inner antenna has an outer diameter of 110 mm and a length of 192.7 mm.

The annular helicon propellant distributor is a sealed stainless steel diffuser with inlets on the rear, and 30 holes of 0.39 mm diameter to distribute propellant into the ionization chamber. The inner diameter of the propellant distributor is 130 mm, and the outer diameter is 160 mm, and the depth is 25.4 mm.

RF power is provided to each antenna in phase via the RF power system. The antennas can be wired with the same or opposite current directions, and are set such that the legs twist are on top of one another, which allows for

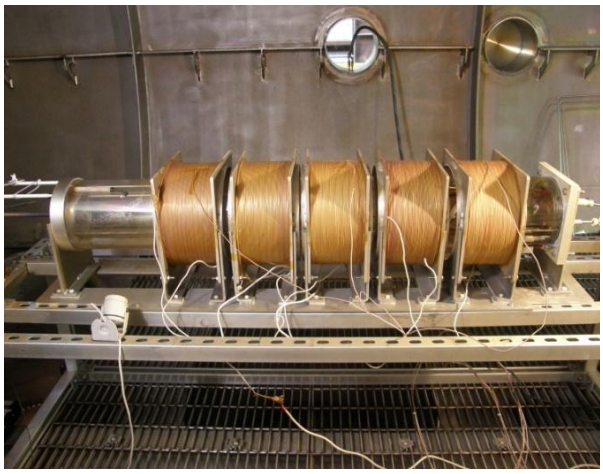

Figure 2. Annular helicon plasma source.

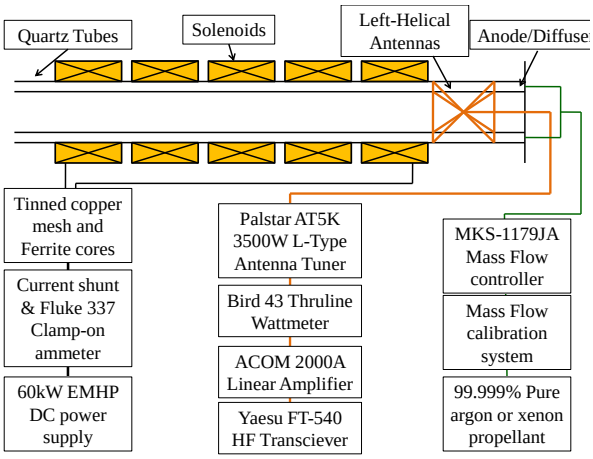

Figure 3. Schematic of Annular Helicon subsystems.

the best coupling of the antennas to the plasma.[21] Annular helicon theory and past experimental studies show that in-phase antennas with current flow in the same direction produces the best coupling to the plasma. The annular helicon requires power for the inner and outer antennas as well as to the magnet solenoids. The RF power input leads connect at the downstream end of each helical antenna and the return leads connect at the upstream end. The antenna leads carry current in the same direction. The antennas are aligned such that the legs twist on top of one another, which allows for optimal coupling of the antennas to the plasma.

Five solenoids, powered by a 60-kW EMHP DC power supply, generate a steady-state axial magnetic field up to 450 Gauss. The power leads to the antennas and solenoids are EMI shielded with tinned copper mesh to eliminate RF radiation into and out of the wiring. ½" and ¼" diameter ferrites reduce RF signal propagation up the power leads.

The Acom 2000A linear amplifier produces RF power up to 2500 W steady state. The RF forward and reflected power levels are measured with a Bird 43 Thruline wattmeter and the Palstar AT5K matching network internal power gauge. The Bird 43 Thruline wattmeter has an accuracy of ±5% of full scale, while the Palstar AT5K wattmeter has an accuracy of ±10% of full scale. The RF power system is enclosed in a Faraday cage to prevent RF radiation from the system components. The cabinet is cooled through EMI shielded ports and is grounded to the vacuum chamber.

The Palstar AT5K 3500 W L-Type matching network, which has a native impedance of 50 Ω, matches the impedance of the amplifier to the load. The impedance of the antennas is extremely low and purely resistive, meaning no inductive reactance is present. For this antenna configuration, the resistance is approximately 3 Ω without plasma present. To minimize radiation outside of the antenna and ionization channel, *i.e.*, reduce reflected and lost power, the impedance of all cabling and feedthroughs is 50 Ω. In addition, a standard fixed distance is maintained between all conductors. The RF reflected power is less than 1% of the forward power for all measurements taken, indicating the antenna is well-tuned to the matching network.

High purity (99.9995% pure) argon or xenon gas is fed through an MKS 1179JA mass flow controller through stainless steel feed lines to the propellant distributor. A custom fixed volume mass flow calibration system is employed to ensure proper flow rates from the mass flow controller. The mass flow controller has an accuracy of ±1% of full scale.

C. Hiden Analytical Langmuir Probe

All ion number density, electron temperature and electron energy distribution function (EEDF) measurements are taken with the Hiden ESPION Langmuir probe system. Chen shows this system is suitable for use in high-density magnetized RF plasma measurements.[26] Figure 4 shows the Hiden ESPION system. The probe has an error of ± 50% for electron number density and ±20% for electron temperature.[26] The probe features a compensation electrode tuned to remove RF signals throughout the 2 – 15 MHz RF frequency range used in these tests. The probe is mounted to a 1.5 m by 1.5 m Parker Daedel automated motion control system to provide linear axial and radial motion with an accuracy of ±1 μm. A 0.15 mm diameter, 10 mm length tungsten probe tip is used as a current collector. A reference electrode is position behind the filament, providing a return path for current collected from the plasma if enabled by the sotware. This corrects measurements for changes in the plasma potential relative to the system ground potential.[27] The probe filament is mounted to the end of an 810 mm long ceramic sting, which contains the RF-compensation inductors. The inductors are cooled through the umbilical with a forced air system. The Hiden software, connected to the control head, collects I-V curves from the plasma. Figure 5 shows a sample Langmuir probe I-V trace. The Hiden ESPION system contains a data analysis tool that uses Orbital-Motion Limited (OML) and Allen, Boyd and Reynolds analysis techniques. Chen recommends using very thin probes, where the probe tip radius is no larger than three times the Debye length, so that OML theory may be used.[28] All diagnostic equipment is grounded to its own separate ground within the facility to prevent RF interference in measurements.

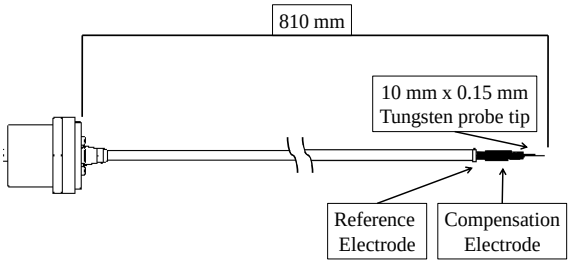

Figure 4. Hiden ESPION Langmuir probe schematic.

1. Langmuir Probe Theory

OML theory uses the fact that ion collection current is independent of the the plasma potential, assuming the current is only limited by the angular momentum of the ions about the probe, and that there exists a sheath edge outside of which the energy distribution is Maxwellian.[27] Figure 6 shows a schematic of the OML sheath and an absorption boundary.[18] OML theory provides a simple relationship for ion current. Eqn. (2) shows this relationship.[18]

$$I \xrightarrow[T_i \to 0]{} A_p ne \frac{\sqrt{2}}{\pi} \left(\frac{|eV_p|}{M} \right)^{1/2} \tag{2}$$

To analyze the raw I-V data, the square root of the ion current fit is added to the original I-V curve to obtain a characteristic, which consists of electron current only.[27] The natural logarithm of the electron current is calculated and plotted against the bias voltage. Eq. 3 calculates the electron temperature by fitting a line to the linear transition region.[18] The relationships for electron temperature and electron number density are shown in Equations (3) and (4).[27]

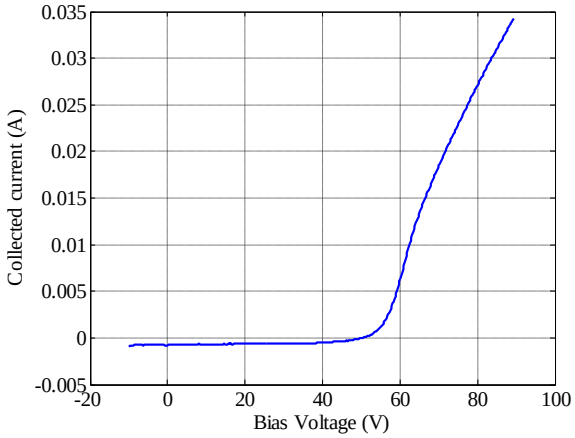

Figure 5. Measured I-V characteristic on argon propellant.

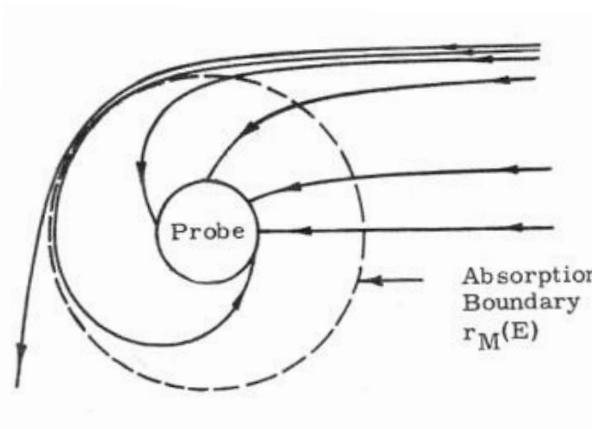

Figure 6. OML theory electron motion near a positively-biased Langmuir probe.[18]

$$T_e = \frac{-1}{slope(I)} \tag{3}$$

$$n_e = 3.73x10^{13} \frac{I_{es(amps)}}{A_{p(m^2)} \sqrt{T_{e(eV)}}} \tag{4}$$

2. Druyvesteyn Method for EEDF Calculation

The Druyvesteyn method is used to calculate the EEDF from the I-V characteristics.[29] The Druyvesteyn method observes that the second derivative of the electron current with respect to the probe potential is proportional to the electron energy distribution function if the velocity distribution is isotropic. Eq. 5 shows this relationship.[30]

$$f_e(E) = \frac{-4}{A_p e^2} \left(\frac{m_e (V_{plasma} - V)}{2e} \right)^{1/2} \frac{d^2 I_e}{dV^2} \tag{5}$$

If the EEDF is Maxwellian, Eq. 5 can be integrated twice to give the theoretical electron current as a function of probe voltage below the plasma potential. Eq. 6 shows the result of these integrations.[30]

$$I_e(V) = \left(eA_p N \sqrt{\frac{kT_e}{2\pi m_e}} \right) \exp\left(\frac{-e(V_{plasma} - V)}{kT_e} \right) \quad (6)$$

The calculation of the EEDF is performed automatically in the Hiden software, and is accurate to ±50%.[27] The second derivative method requires a smooth I-V trace to produce accurate results.[30] Any increases in the second derivative can produce false peaks in the EEDF. To allow numerical integration, each I-V trace is taken at 0.1 V resolution from -15 V to 90 V. Ten I-V traces per operating point are collected and the average of the ten traces is used as an input to the Druyvesteyn method. This method of data analysis is supported by Hiden.[27] The EEDF contained outlying points above the 10 eV level, however these were on the order of 2% of the peak value and are truncated.

III. Experimental Data

The annular helicon plasma source is characterized over a broad range of operating conditions. Axial profiles of ion number density and electron temperature are important to determine the optimal location for mating to a HET. Radial profiles of ion number density and electron temperature are important to measure to ensure a HET located in the exhaust of the helicon will receive uniform high density plasma for acceleration. RF power profiles have been shown to indicate mode shifts within the plasma. Therefore, RF power profiles are taken at several operating conditions to determine a threshold for reaching an observed mode shift. RF frequency profiles are taken to determine if the annular helicon is tunable to a given propellant. If an optimal RF frequency exists for a given propellant, this may allow the annular helicon to be used to ionize a multitude of propellants. The downstream portion of the antenna is located at an axial location of 0 mm. The exhaust plane of the device is at an axial location of 480 mm.

A. Axial Profile

Figures 7 and 8 show an axial profile of the ion number density and electron temperature with argon propellant. These measurements are taken along the centerline of the annular channel, at the top center of the exhaust plane. Figures 7 and 8 indicate differences between the trends of the 400 Gauss magnetic field to the lower magnetic field cases. For the zero and 200 Gauss magnetic field cases, the ion number density increases as the distance from the antenna increases, rising from 4.4 x 10^{16} m^{-3} to a peak of 1.3 x 10^{17} m^{-3}. For the 400 Gauss magnetic field, the ion number density starts at a higher level than the lower magnetic field cases (1.7 x 10^{17} m^{-3}), and decreases as the distance from the antenna increases. The 400 Gauss magnetic field case has the lowest electron temperatures with an average of 2.5 eV, while the 200 Gauss magnetic field case has the highest, with an average of 5.7 eV. The electron temperature values vary along with the ion number density, i.e., the increase in ion number density is accompanied by an increase in electron temperature.

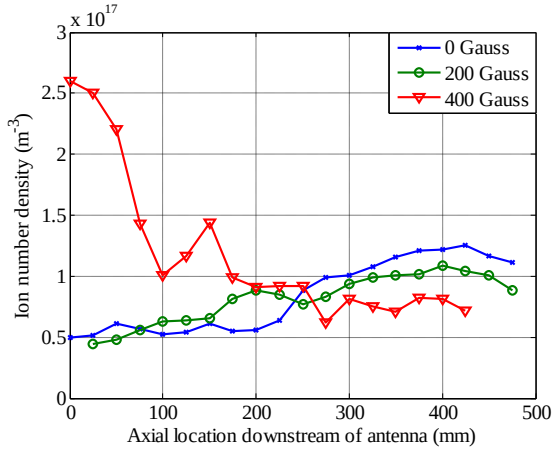

Figure 7. Ion number density versus axial location. *7 MHz RF frequency, 1 kW RF forward power, 3 mg/s Ar mass flow rate, 3.0 x 10^{-5} Torr-Ar operating pressure.*

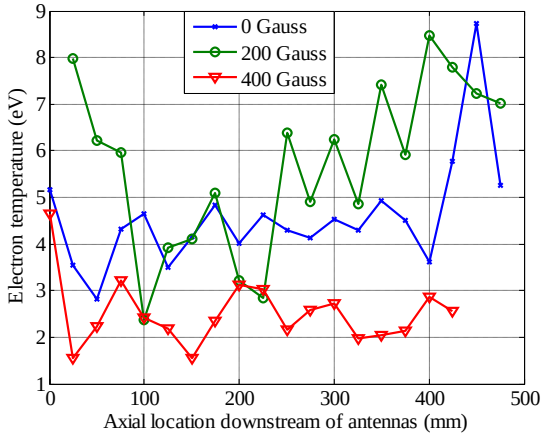

Figure 8. Electron temperature versus axial location. *7 MHz RF frequency, 1 kW RF forward power, 3 mg/s Ar mass flow rate, 3.0 x 10^{-5} Torr-Ar operating*

B. Radial profile

Figures 9 and 10 show radial profiles of the ion number density and electron temperature with argon propellant. These measurements are taken at an axial location of zero mm, at the right center of the exhaust plane as viewed from downstream. The inner wall of the annulus is located at a radial location of 0 mm, while the outer wall of the annulus is at a radial location of 21.5 mm.

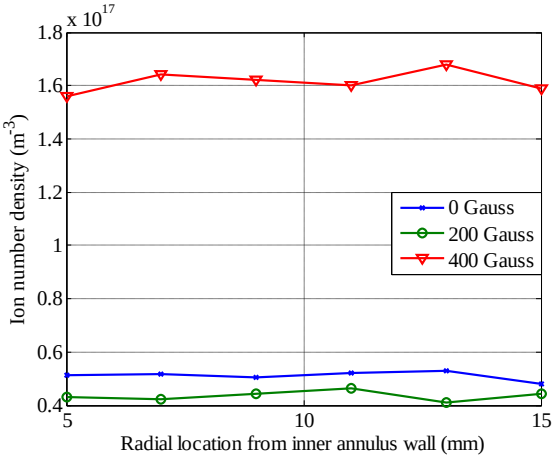

Figure 9. Ion number density versus radial location. *Zero mm axial location, 7 MHz RF frequency, 1 kW RF forward power, 3 mg/s Ar mass flow rate, 3.0 x 10^{-5} Torr-Ar operating pressure.*

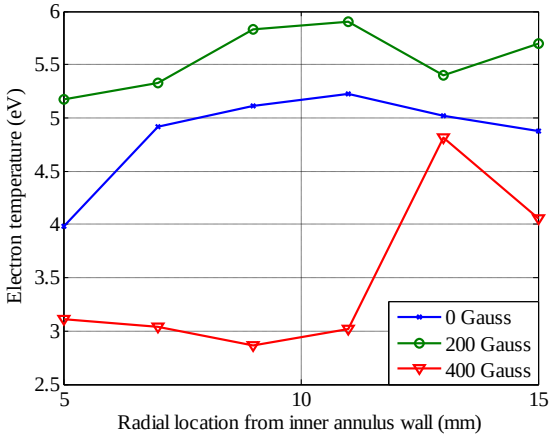

Figure 10. Electron temperature versus radial location, *Zero mm axial location, 7 MHz RF frequency, 1 kW RF forward power, 3 mg/s Ar mass flow rate, 3.0 x 10^{-5} Torr-Ar operating pressure.*

Figures 9 and 10 show the increased ion number density that can be reached at an axial location of zero mm in the 400 Gauss magnetic field strength case. The ion number density increases by a factor of 10 or more at this magnetic field strength, peaking at 1.6 x 10^{17} m^{-3} for the 400 Gauss case. The lowest electron temperatures measured are for the 400 Gauss case, at a value of 2.8 eV, while the highest are in the 200 Gauss case, at 5.9 eV.

C. RF power profile

Figures 11 and 12 show the ion number density and electron temperature as a function of RF power. These measurements are taken at an axial location of 250 mm, on the channel centerline, using argon propellant. This location is the just downstream of the antennas and is the

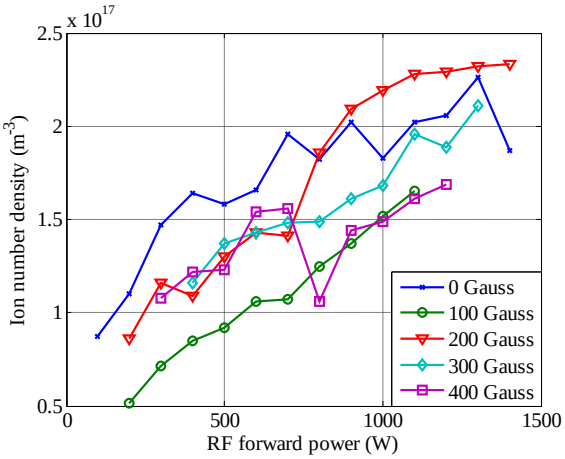

Figure 11. Ion number density versus RF forward power. *250 mm downstream of antennas, 7 MHz RF frequency, 3 mg/s Ar mass flow rate, 3.0 x 10^{-5} Torr-Ar operating pressure.*

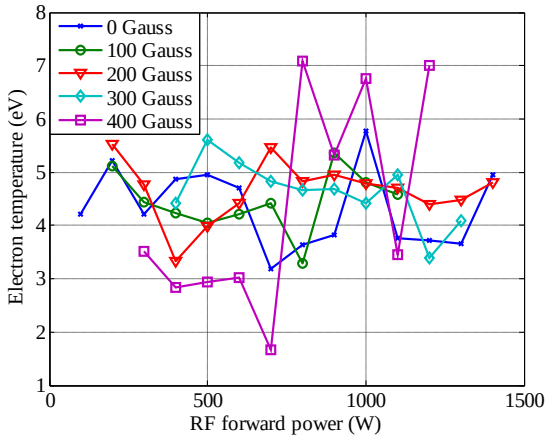

Figure 12. Electron temperature versus RF forward power. *250 mm downstream of antennas, 7 MHz RF frequency, 3 mg/s Ar mass flow rate, 3.0 x 10^{-5} Torr-Ar operating pressure.*

location for the highest ion number density from previous investigations.[22]

The zero Gauss magnetic field case exhibits the highest ion number density at power levels less than 800 W, after which the 200 Gauss case trends highest, with a peak of 2.3 x 10^{17} m^{-3}. The remaining ion number densities follow similar trends and are between 5.1 x 10^{16} m^{-3} and 3.5 x 10^{17} m^{-3}. The 400 Gauss case has the lowest electron temperature at 1.6 eV, as well as the highest at 7.0 eV.

D. RF frequency profile

Figures 13 and 14 show the ion number density and electron temperature as a function of RF frequency. These measurements are taken at an axial location of zero mm, on the channel centerline, using argon propellant. Figures 6 shows this location is the peak ion number density for the highest magnetic field case.

These measurements show ion number densities within 13% of the average of 1.2 x 10^{17} m^{-3} for the 500 W RF power case. The 1000 W RF power case shows similar trends, however between 7 and 9 MHz, and again at 12 MHz, the ion number density is significantly higher, peaking at 1.9 x 10^{17} m^{-3} at 8 MHz.

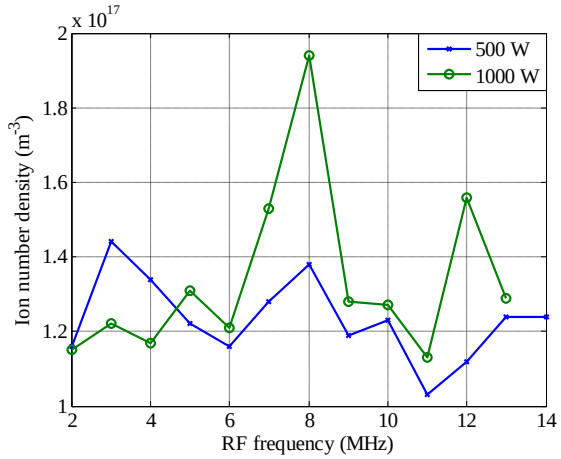

Figure 13. Ion number density versus RF frequency. *Zero mm downstream of antennas, 1 kW RF forward power, 400 Gauss B-field, 3 mg/s Ar mass flow rate, 3.0 x 10^{-5} Torr-Ar operating pressure.*

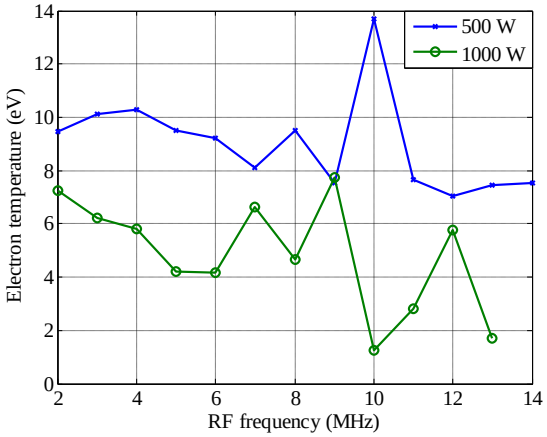

Figure 14. Electron temperature versus RF frequency. *Zero mm downstream of antennas, 1 kW RF forward power, 400 Gauss B-field, 3 mg/s Ar mass flow rate, 3.0 x 10^{-5} Torr-Ar operating pressure.*

E. Electron Energy Distribution Functions

Figure 15 shows the EEDF at several selected RF frequencies. These measurements are taken at an axial location of zero mm, on channel centerline, 1 kW RF power, at a magnetic field strength of 400 Gauss. This axial location is selected as it is the peak ion number density from Figure 6. Figure 14 shows that the peak of the EEDF can be manipulated for a given propellant by selection of the RF frequency. The peak of the EEDF varies from as low as 2.0 eV to as high as 4.7 eV for the operating points tested.

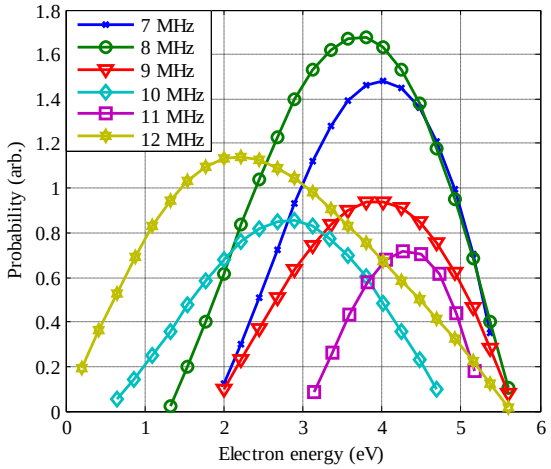

Figure 15. EEDF at selected RF frequencies. *Zero mm downstream of antennas, 1 kW RF forward power, 400 Gauss B-field, 3 mg/s Ar mass flow rate, 3.0 x 10^{-5} Torr-Ar operating pressure.*

F. Xenon axial profile

Figures 16 and 17 show axial profiles of the ion number density and electron temperature for xenon propellant. These measurements are taken at a radial location on channel centerline, at a magnetic field strength of 200 Gauss, and are compared to that of argon

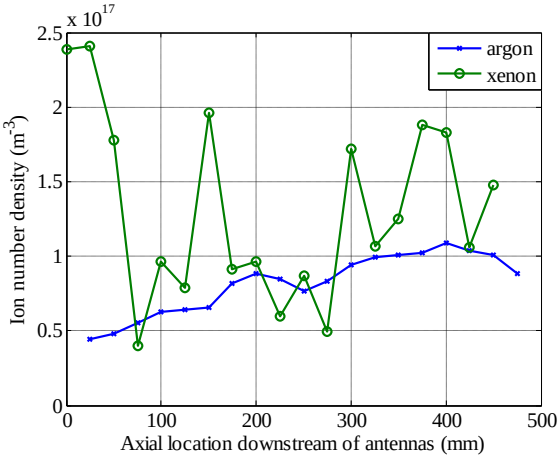

Figure 16. Ion number density versus axial location. *7 MHz RF frequency, 1 kW RF forward power, 200 Gauss B-field, 3 mg/s mass flow rate argon and xenon, along channel centerline, 3.0 x 10^{-5} Torr-Ar operating pressure, 5.6 x 10^{-5} Torr-Xe operating pressure.*

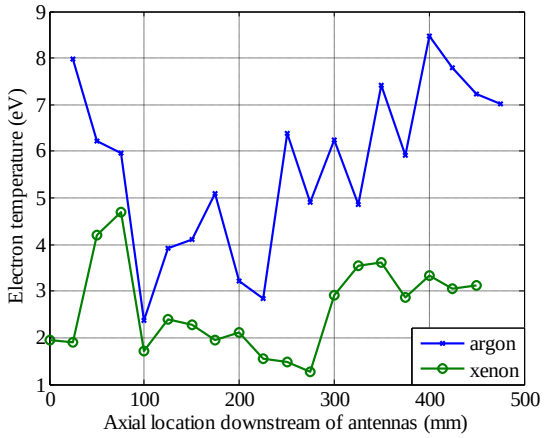

Figure 17. Electron temperature versus axial location. *7 MHz RF frequency, 1 kW RF forward power, 200 Gauss B-field, 3 mg/s mass flow rate argon and xenon, along channel centerline, 3.0 x 10^{-5} Torr-Ar operating pressure, 5.6 x 10^{-5} Torr-Xe operating pressure.*

from Figure 6. Figures 15 and 16 show increased ion number densities and electron temperatures for xenon over argon, reaching a peak value of 2.4 x 10^{17} m^{-3} for xenon and 1.2 x 10^{17} m^{-3} for argon. Xenon also reaches much higher electron temperatures, peaking at 8.4 eV for xenon and 4.8 eV for argon. Xenon trends are much noisier than those of argon. Xenon exhibits electron temperatures that are on average 55% lower, and ion number densities that are on average 41% higher than those of argon at the same operating conditions.

IV. Discussion

The RF compensated Langmuir probe data gathered establishes a baseline for annular helicon plasma generation across the range of operating conditions measured. The trends in the data are now examined to determine their correlation with previous results, as well as coupling modes observed and appropriateness of this plasma source as a ionization stage of a HET.

In order to understand the mechanisms behind the trends indicated in the measurements, plasma parameters are calculated for each trend. These include the electron and ion cyclotron frequencies ω_{ic}, ω_{ec}, and plasma parameter Λ.

The plasma parameter Λ, which is a measure of the population of the Debye sphere, is calculated to be on the order of 10^{-24} for all measurements taken. This indicates the Debye sphere is sparsely populated, corresponding to strongly coupled plasma. The gyroradii calculations for measurements with argon indicate the electrons are magnetized for the 200 and 400 Gauss magnetic field cases, but the ions are not.

Table 3 shows the electron and ion cyclotron frequencies calculated from the axial ion number density and electron temperature profiles shown in Figures 6 and 7.[30]

Table 3. Electron and ion cyclotron frequencies.

	200 Gauss	**400 Gauss**
Electron cyclotron frequency (Hz)	3.5 x 10^{9}	7.0 x 10^{9}
Ion cyclotron frequency (Hz)	4.8 x 10^{4}	9.6 x 10^{4}

The axial ion number density trends shown in Figures 7 and 8 indicate there is a different coupling mechanism at 400 Gauss magnetic field strength than the zero or 200 Gauss cases. The dependence of the ion number density on magnetic field could indicate a helicon wave mode is being excited due to the magnetic field coupling to the RF. However, the ion number densities are lower than most helicon modes are known to excite, so the perpendicular and parallel wave numbers must be ascertained by B-dot probe measurements. The power density for this device is at maximum 4.3 x 10^{4} W/m^{3}, which is comparable to similar cylindrical helicon devices.[25, 31] This indicates that the decrease in ion number density is not attributable to a lack of power density. The electron temperature profiles show the higher ion number density cases trending towards the lowest electron temperatures, which is the most efficient

method as the most percentage of input energy is going into ionization rather than electron energy. The zero and 200 Gauss magnetic field cases trend towards highest electron temperatures, especially near the exit plane of the device.

The RF forward power profiles shown in Figures 11 and 12 indicate the highest ion number densities can be reached in the zero Gauss configuration, up to 2.4 x 10^{17} m^{-3}. Each sweep indicates an increase in ion number densities with RF forward power, and shows that the magnetic field does not make a significant impact on the ion number density in this coupling mode. This leads us to believe the RF power profiles observed are not helicon wave modes as the magnetic field has no effect on the ion number density. The electron temperatures measured fall between 3 eV and 6 eV, with the exception of the noisy 400 Gauss magnetic field case, which spikes to above 7 eV at RF power levels above 700 W. These data points are likely exaggerated by the probe feeding current to the plasma. At high bias voltages, Hiden has shown the probe can emit it's own electrons, as well as generate a ground loop within the plasma.[27] Without accompanied increases in ion number density, the jumps in electron temperature do not indicate a shift to helicon mode.

The RF frequency trend shown in Figures 13 and 14 is critical to understanding the benefits of a helicon device over other ionization options. For a given propellant, there exists an optimal frequency at which the annular helicon will produce a maximum ion number density. The RF frequency trend shows that for argon propellant, the highest ion number density of 1.9 x 10^{17} m^{-3} is produced at 8 MHz for the 1000 W case, whereas for the 500 W case, the ion number density is slightly lower (an average of 1.4 x 10^{17} m^{-3}) and is independent of RF frequency. This indicates a different coupling mode for the high power case.

The EEDFs measured indicate a single-hump structure for most measurements taken. EEDF trends measured in Figure 16 indicate the EEDF varies by selection of RF frequency. The lower RF frequencies measured tend towards higher peaks in the EEDF, however at 10 and 12 MHz, the EEDF peak shifts lower, which produces lower energy electrons. The 10 MHz and 12 MHz cases exhibit the broadest EEDFs measured, while the 7 MHz case shows the narrowest range of electron energies.

Figure 18 shows the electron-argon impact ionization cross section as a function of impact electron energy. This may be related to the EEDF peak value and probability distribution. In this case, the peak electron energy is from the 11 MHz case, while the minimum is in the 12 MHz case. While the ionization cross-section data would indicate the 12 MHz case should have much lower ion number density than the 11 MHz case, in fact the opposite is true. This indicates that electron-argon cross section is not the only parameter useful in prediction of ion number density trends in the coupling modes observed. Weak coupling can cause higher electron temperatures and lower ion number densities despite a larger electron-argon cross section. Figure 18 shows the optimal average electron energy for maximization of the argon-electron ionization cross section is 14 eV. While an average electron energy of 14 eV is unusual in most cylindrical helicons, Figure 19 shows the optimal average electron energy for xenon is 5 eV. This average electron energy is very common in most helicons.

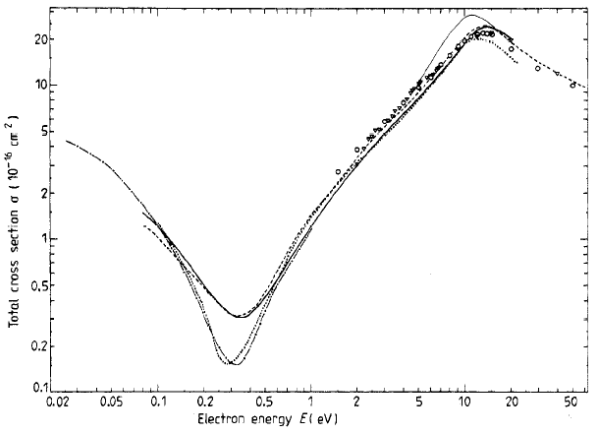

Figure 18. Electron-argon ionization cross section versus electron energy. [32]

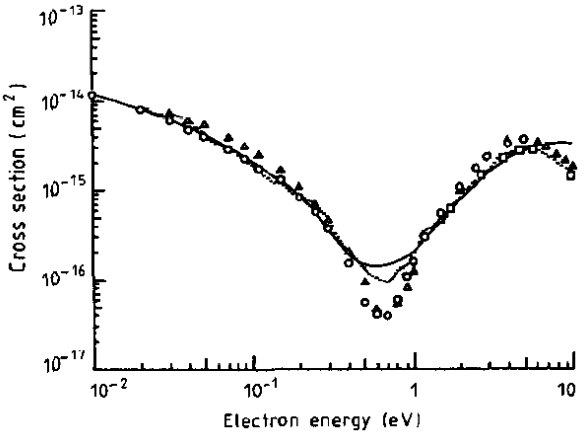

Figure 19. Electron-xenon ionization cross section versus electron energy. [33]

Figures 16 and 17 compare the ion number density axial trends for both argon and xenon. While the argon trends are smooth, the xenon case shows higher ion number densities of up to 2.5 x 10^{17} m^{-3}, but is much more uneven. The xenon electron temperatures are significantly lower than those of argon, indicating xenon plasma is more strongly coupled. The lower electron temperature and higher ion number density for xenon can be attributed to more complete ionization due to the lower ionization energy of the xenon, 12.1 eV for xenon as opposed to 15.7 eV for argon.

The optimal location to mate a Hall thruster is at the

antenna exit plane, which also minimizes device size, therefore weight. At this location, the plasma also has the highest ion number density and lowest electron temperature for xenon and argon propellants.

V. Conclusion

The peak ion number density recorded for argon is 3.5 x 10^{17} m^{-3}, at a location zero mm downstream of the antennas, at an RF frequency of 7 MHz, RF forward power of 1300 W, and a magnetic field of 0 Gauss. Peak ion number density for xenon is 2.5 x 10^{17} m^{-3}, which occurs at a location zero mm downstream of the antennas, at an RF frequency of 7 MHz, RF forward power of 1000 W, at a magnetic field of 200 Gauss. Axial profiles of ion number density show a different coupling mode is excited at a magnetic field strength of 400 Gauss for an otherwise identical operating condition. This indicates the coupling mode is a helicon wave mode, as there is magnetic field dependence. RF frequency profiles show that 8 MHz is the optimal frequency for argon propellant to maximize the ion number density. The EEDF is calculated for several RF frequencies and it is shown the peak and width of the EEDF varies by selection of the RF frequency for a given propellant. Xenon propellant yields the highest ion number densities at the lowest electron temperatures. The annular helicon produces high density plasma with a constant radial profile at an axial location of zero mm. At this location, the maximum density plasma will be ejected into the HET acceleration stage of the proposed two stage annular helicon closed drift thruster.

Acknowledgments

The authors wish to thank the Marshall Space Flight Center for supplying the RF power system, Scott Elliott and Scott Moseley of the Georgia Tech Aerospace Engineering Machine Shop for fabrication of hardware. This research is supported by the Air Force Office of Scientific Research grant FA9550-07-1-0137. Dr. Mitat Birkan is the contract monitor.

References

1. Hofer, R.R., Jankovsky, R. S. . "A Hall Thruster Performance Model Incorporating the Effect of a Multi-Charged Plasma," AIAA-2001-3322, *37th Joint Propulsion Conference and Exhibit*, Salt Lake City, UT, July 8-11, 2001.
2. Beal, B.E., Gallimore, A. D., Morris, D. P., Davis, C., Lemmer, K. M. "Development of an Annular Helicon Source for Electric Propulsion Applications," AIAA-2006-4841, *42nd Joint Propulsion Conference and Exhibit*, Sacramento, CA, July 8-11, 2006.
3. R. R. Hofer, P.Y.P., A. D. Gallimore. "A High Specific Impulse Two-Stage Hall Thruster with Plasma Lens Focusing," *27th International Electric Propulsion Conference*, Pasadena, CA, October 15-19, 2001.
4. Jacobson, D.T., Jankovsky, R. S., Rawlin, V. K., Manzella, D. H. "High Voltage TAL Performance," AIAA-2001-3777, *37th Joint Propulsion Conference and Exhibit*, Salt Lake City, UT, July 8-11, 2001.
5. Beal, B.E., Gallimore, A. D. "Development of the Linear Gridless Ion Thruster," AIAA-2001-3649, *37th Joint Propulsion Conference and Exhibit*, Salt Lake City, UT, July 8-11, 2001.
6. Fruchtman, A., Fitsch, N. J., Raitses, Y. . "Hall Thruster with Absorbing Electrodes," AIAA-2000-3659, *36th Joint Propulsion Conference and Exhibit*, Huntsville, AL, July 16-19, 2000.
7. Solodukhin, A.E., Semenkin, A. V. , Tverdohlebov, S. O. , Kochgerin, A. V. . "Parameters of D-80 Anode Layer Thruster in One- and Two-Stage Operation Modes," IEPC-2001-032, *27th International Electric Propulsion Conference*, Pasadena, CA, Oct. 15-19, 2001.
8. Pote, B., Tedrake, R. "Performance of a High Specific Impulse Hall Thruster," IEPC-2001-35, *27th International Electric Propulsion Conference*, Pasadena, CA, Oct. 15-19, 2001.
9. Hofer, R., "Development and Characterization of High-Efficiency, High-Specific Impulse Xenon Hall Thrusters," Ph.D. Thesis, The University of Michigan, Dept. of Aerospace Engineering, Ann Arbor, MI, 2004
10. Szabo, J., Warner, N., Martinez-Sanchez, M. "Instrumentation and Modeling of a High Specific Impulse Hall Thruster," AIAA-2002-4248, *38th Joint Propulsion Conference and Exhibit*, Indianapolis, IN, July 7-10, 2002.

11. Fisch, N.J., Raitses, Y., Litvak, A. A., Dorf, L. A. "Design and Operation of Hall Thruster with Segmented Electrodes," AIAA-99-2572, *35th Joint Propulsion Conference and Exhibit*, Los Angeles, CA, July 7-10, 1999.
12. Fisch, N.J., Raitses, Y. , Litvak, A. A., Dorf, L. A. "Segmented Electrode Hall Thruster Operation in Single and Two Stage Regimes," IEPC-99-101, *26th International Electric Propulsion Conference*, Kitakyushu, Japan, Oct. 17-21, 1999.
13. Fisch, N.J., Raitses, Y., Litvak, A. A., "Variable Operation of Hall Thruster with Multiple Segmented Electrodes," Journal of Applied Physics, Vol. 89, No. 4, Feb., 2001, pp.2040-2046.
14. Molina-Morales, P., Kuninaka, H., Toki, K., Arakawa, Y. "Preliminary Study of an ECR Discharge Hall Thruster," IEPC-2001-069, *27th International Electric Propulsion Conference*, Pasadena, CA, Oct. 15-19, 2001.
15. Chen, F.F., "Plasma Ionization by Helicon Waves," Plasma Physics and Controlled Fusion, Vol. 33, No. 4, 1991, pp.339-364.
16. Chen, F.F. "Helicon Wave Plasma Sources," *Proceedings of the International Conference on Plasma Physics*, Kiev, USSR, 1987.
17. Chi, K.-K., Sheridan, T. E., Boswell, R. W., "Resonant cavity modes of a bounded helicon discharge," Plasma sources Science and Technology, Vol. 8, No. 3, 1999, pp.421-431.
18. Chen, F.F. "RF Langmuir Probes, revisited," *58th Gaseous Electronics Conference*, San Jose, CA, 2005.
19. V. V. Zhurin, H.R.K., R. S. Robinson, "Physics of Closed Drift Thrusters," Plasma Sources Sci. Technology, Vol. 8, No. 1, 1999, pp.R1-20.
20. Yano, M., Walker, M. L. R., "Plasma Ionization by Annularly-Bounded Helicon Waves," Physics of Plasmas, Vol. 13, No. 6, June, 2006, pp.1-5.
21. Yano, M., Palmer, D, Williams, L, Walker, M. L. R. "Design and Operation of an Annular Helicon Plasma Source," AIAA-2007-5309, *43rd Joint Propulsion Conference*, Cincinatti, OH, July 8-11, 2007.
22. Palmer, D., Akinli, C., Walker, M. L. R. "Characterization of an Annular Helicon Plasma Source," IEPC-2007-202, *30th International Electric Propulsion Conference*, Florence, Italy, September 17-20, 2007.
23. *Vacuum Measurement*, Varian, Inc., 2005, Available from: http://www.varianinc.com/cgi-bin/nav?products/vacuum/measure/index&cid=IPMHIKJQFO.
24. Randolph, T., Kim, V., Kaufman, H., Kozubsky, K., Zhurin, V. V., Day, M. ""Facility Effects on Stationary Plasma Thruster Testing"," IEPC-93-093, *23rd International Electric Propulsion Conference*, Seattle, WA, Sep. 13-16, 1993.
25. West, M., Charles, C., Boswell, R., "Testing a Helicon Double Layer Thruster Immersed in a Space-Simulation Chamber," Journal of Propulsion and Power, Vol. 24, No. 1, Jan. - Feb., 2008, pp.134-141.
26. Chen, F.F., "Langmuir probe analysis for high density plasmas," Physics of Plasmas, Vol. 8, No. 6, 28 February, 2001.
27. *Handbook of Plasma Diagnostics*, Hiden Analytical Limited, 2000.
28. Chen, F.F. Use of Langmuir probes in RF plasmas. *INER*. 2008. Taiwan.
29. Druyvestyn, M.J., "Der Neidervoltbogen," Z Phys A Hadrons and Nuclei, Vol. 64, No., 1930, pp.781-798.
30. Herman, D., "The Use of Electrostatic Probes to Characterize the Discharge Plasma Structure and Identify Discharge Cathode Erosion Mechanisms in Ring-Cusp Ion Thrusters," Ph.D. Thesis, The University of Michigan, Dept. of Aerospace Engineering, Ann Arbor, MI, 2005
31. Sudit, I.D., Chen, F. F., "RF compensated probes for high-density discharges," Plasma Sources Science and Technology, Vol. 3, No. 2, May, 1994, pp.162-168.
32. Ferch, J., Granitza, B., Masche, C.,Raith, W., "Electron-argon total cross section measurements at low energies by time-of-flight spectroscopy," Journal of Physics B, Vol. 18, No. 5, 1985, pp.967-983.
33. Suzuki, M., Taniguchi, T., Yoshimura, N., Tagashira, H., "Momentum Transfer cross section of xenon deducted by electron drift data," Journal of Physics D: Applied Physics, Vol. 25, No. 1, 1992, pp.50-56.